

## Robust Control of a Medium Voltage AC/DC Testbed

C. Tschritter\*, A.N. Johnston\*, L. Vu<sup>‡</sup>, T. Nguyen<sup>‡</sup>, D.A. Wetz\*, T.V. Vu<sup>‡</sup>, K. Schoder<sup>‡</sup>, J. Langston<sup>‡</sup>, H. Ravindra<sup>‡</sup>, M. Stanovich<sup>‡</sup>, M. Steurer<sup>‡</sup>, C.M. Schegan<sup>+</sup>, and J.M. Heinzl<sup>+</sup>

\* *Univ. of Texas at Arlington (UTA), Arlington, TX USA*

<sup>‡</sup> *Clarkson University, Potsdam, NY USA*

<sup>‡</sup> *Florida State University, Center for Advanced Power Systems, Tallahassee, FL USA*

<sup>+</sup> *Naval Surface Warfare Center - Philadelphia, Philadelphia, PA USA*

\* Corresponding Author. Email: [wetz@uta.edu](mailto:wetz@uta.edu)

### Synopsis

Future shipboard power systems are likely to employ multiple generation sources that are monitored and autonomously controlled. Energy storage may be used to backup and buffer traditional generation sources during down times or when transient loads are deployed. Coupling intelligent control with energy storage will ensure that efficiency, reliability, and power quality can be maintained. At the University of Texas at Arlington (UTA), a hardware testbed has been installed to study one zone of a conceptual power system architecture. It has AC and DC distributed power sources operating in the few hundreds of kW range and loads at 4160 VAC, 480 VAC, 1 kVDC, 6 kVDC, and 12 kVDC respectively. Transient loads are emulated by modulating the installed power sources into resistive load banks. UTA is collaborating with Clarkson University (CU) and Florida State University (FSU) to extend the testbed virtually using a hardware in the loop (HIL) platform and to demonstrate robust power system control using Simulink desktop real-time. This paper will discuss the collaborative efforts and provide some results collected.

Keywords: Microgrid; Medium-Voltage Power Distribution; Power System Control; Power Electronics; Energy Storage

### 1. Introduction

The first electrification of ships dates to 1903 in the Vandal with the introduction of diesel electric propulsion, but it wasn't until the 1920s that the first generation of electric ships utilizing electric propulsion drives were manufactured. These ships had steam turbine generators that powered the propeller motors and varied the propeller motor speed by varying the generator speed (Hansen 2015); however, they soon began to disappear as diesel engines became predominant within the industry. It wasn't until power electronic devices emerged in the 1980s that the resurgence of the all-electric ship concept resurfaced and then gained traction with the development of

variable speed drives (VSDs) in the 1990s (Ortiz 2010). Over time, there have been several studies performed to evaluate shipboard and terrestrial applications of MVAC, MVDC, or combination MVAC/MVDC microgrids. Some examples include cruise vessels, icebreakers, and liquefied natural gas (LNG) tankers that utilize electric propulsion and varying levels of AC and DC loads in either constant or pulsed power operation (ONR 2021). These case studies have shown that there are potential benefits but also drawbacks to incorporating these different microgrid structures.

Much of the discussion in support or opposed to AC and/or DC power systems centers around one of the following, power quality, the size and availability of equipment and components. Since its inception, AC power, and MVAC microgrids by extension, have suffered from issues inherent to this power system arrangement including frequency matching and reactive power compensation. In an MVAC structure, like the one seen in Figure 1, prime movers must be synchronized, and the frequency of these machines must be adjusted to maintain the AC frequency at its required rating (i.e., 60 Hz) regardless of loading conditions. This limits the ability to adjust and optimize the parameters of these machines as loads are stepped on and off and creates a less fuel efficient and more environmentally unfriendly solution. Introducing DC energy storage into an AC distribution system requires AC/DC and DC/AC converters. Rectified generators and machines do not require phase angle synchronization and the previously discussed frequency matching is eliminated leading to the possibility of connecting a diverse set of power sources, energy storage, and loads. These machines also benefit from a reduction in size due to the ability to operate at higher rotational speeds and lower torque while generating a higher power density. They have the capability of optimization where parameters can be calculated instantaneously based upon current loading characteristics and then subsequently adjusted to prevent a voltage unbalance at grid connections. Rectification of poly-phase machines provide a higher quality of rectified DC power, improved reliability, and a lower current rating per phase as opposed to the traditional three phase machines incorporated into many MVAC systems (Javaid 2015).

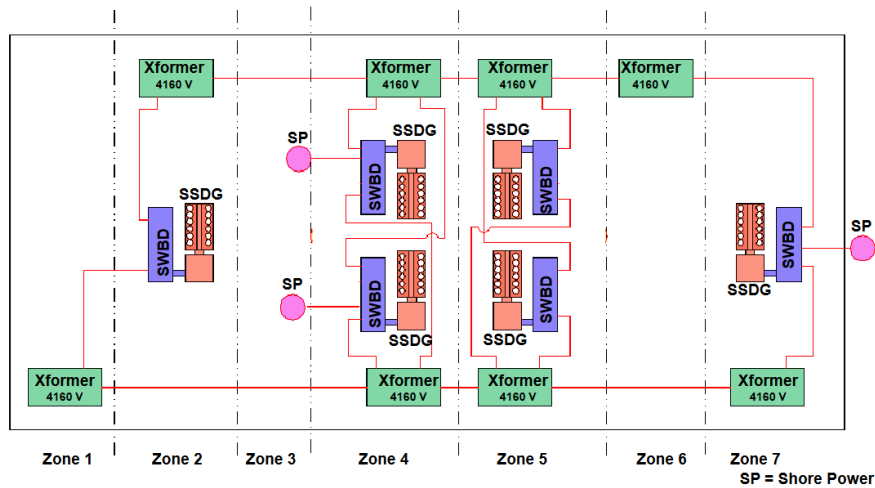


Figure 1: Doerry's MVAC reference architecture (NGIPS 2007).

Depending upon the voltage amplitude, DC power distribution systems provide a slightly easier opportunity for the inclusion of energy storage since it can be floated on the bus if the battery voltage and distribution voltage are well matched. In MVDC systems, the distribution voltage is almost certainly much higher than the energy storage voltage and therefore DC/DC converters are required. Converters stepping up or down DC voltages to MVDC levels are rare and hard to find commercially. Studies have been performed considering the inclusion of many different forms of energy storage including batteries, capacitors, flywheels, and hybrid combinations of these technologies due to their widely varying energy density and power density. Li-ion batteries offer a high combined power and energy density making them very attractive, but they have lifetime and safety concerns that have tempered their use. Supercapacitors offer a high-power density but modest energy density. Batteries and ultracapacitors can serve as both a source or load for the purpose of buffering power quality of connected generators during transient loading operations and this makes them very attractive. High-speed flywheels offer a high combined power and energy density, but they are expensive and, in some cases, difficult to manufacture. Hybrid energy storage systems (ESSs) that employ multiple technologies, in a controlled manner, afford the benefits of each to be realized and they have been evaluated in recent years with great success (Ding 2007).

A shipboard power system architecture employing multiple distributed power sources and power electronic conversion requires a significant level of active monitoring and control to realize its full potential. When energy storage is employed, it buffers traditional generation sources serving as a source to supply the initial transient load

and as a load to the generation sources when load is quickly removed. During transient load buffering, the energy storage can quickly supply load and regulated down slowly while traditional generation sources ramp up. The ramp rate can be adjusted dynamically by the controller depending on the present operating requirements and constraints. If the load exceeds the generation capability, the battery can buffer excess load or the controller can intelligently shed load based off of a priority hierarchy. Real time power system controls are needed to ensure that all the different generation sources and loads are operated in the most reliable and efficient manner. The work performed here is in support of a US Future Naval Capability (FNC) program entitled Robust Combat Power and Energy Cotnrols (RCPC) (Ravindra 2022).

When not enough power generation is available to meet the full load demand, load shedding becomes required. Load shedding is a critical control function in electric ship power systems to ensure the critical load operation under emergency events such as generation losses (Ding 2007, Ravindra 2022, Ding 2006, Xing 2012). Approaches have been conducted to address the load shedding problem during such an unbalanced power event are under-voltage/under-frequency load shedding or schedule load shedding ensuring power balance. The latest effort in (Nguyen 2021) incorporates the varying weighting factors of loads depending on the ship system mission into the objective function to maximize the system operability during the load shedding process. In (Sabah 2021), the authors introduce the evolution of operability-based performance metrics that also uses the weighting factor to assess its impact on system operability. While the previous work have all addressed key aspects of the load shedding problem, they are mostly implemented in the pure simulation platform or controller-hardware-in-the-loop (CHIL) experiments. Realization of hardware implementation is a critical factor in the field demonstration as risks are finally resolved considering hardware limitations. To address this issue, this paper proposes to realize a shedding control reduced scale hardware testbed. The advanced load shedding scheme is incorporated with distinctive features to ensure the safe and realistic hardware implementation. It ensures the power balance between load demands and available generators in a short amount of time to prevent the generator failure and it guarantees the ramp-rate limitation of the hardware system.

The control algorithms employed within a power system along with the latency that exists between the sensors, measurement system, controller, and the physical hardware will play a large role in the ability to optimize power quality, ramp rate support, and load shedding. In the work performed here, researchers at the University of Texas at Arlington (UTA) in Arlington, Texas, Clarkson University (CU) in Potsdam, New York, Florida State University (FSU) in Tallahassee, Florida, and the Naval Surface Warfare Center – Philadelphia Division (NSWC-PD) in Philadelphia, Pennsylvania, have collaborated to demonstrate active load shedding on the Intelligent Distributed Energy Analysis Laboratory (IDEAL) power system testbed installed on the UTA campus. In this report, a brief overview of the IDEAL power system, the Simulink real-time power system controller developed by CU, and some preliminary data collected from their integration will be presented.

## **2. IDEAL Experimental Testbed**

The UTA IDEAL testbed was constructed to emulate a single zone of an MVAC/MVDC electric ship. The testbed includes an electric motor/generator set, multiple AC and DC buses, power converters, transformers, variable resistive loads, and a lithium iron phosphate (LFP) battery. Figure 2 presents an electrical one-line diagram of the testbed and Figure 3 presents a graphical one-line diagram. Figure 2 highlights the capability along with placement of the current and voltage monitoring distributed throughout. It has been previously documented at length (Johnston 2022, Johnston 2020, Johnston 2020, Johnston 2021) though some additions and improvements have been made since those publications were written. The primary source of AC power for the testbed is a Motor-Generator (M-G) set, labelled G1 in Figure 3, controlled by a Variable Frequency Drive (VFD) that supplies 480 VAC and has a maximum power rating of 150 kW. It is a four-pole synchronous generator with rotational frequency of 1500 – 2000 rpm controlled using a four-pole 300 hp induction motor. Using two independent analog reference signals, the generator's output voltage can be altered by +/- 20% and its frequency, via control of the VFD, can be altered between 50 to 67 Hz. With this capability, alternative generation sources are emulated through model execution on a real-time simulator.

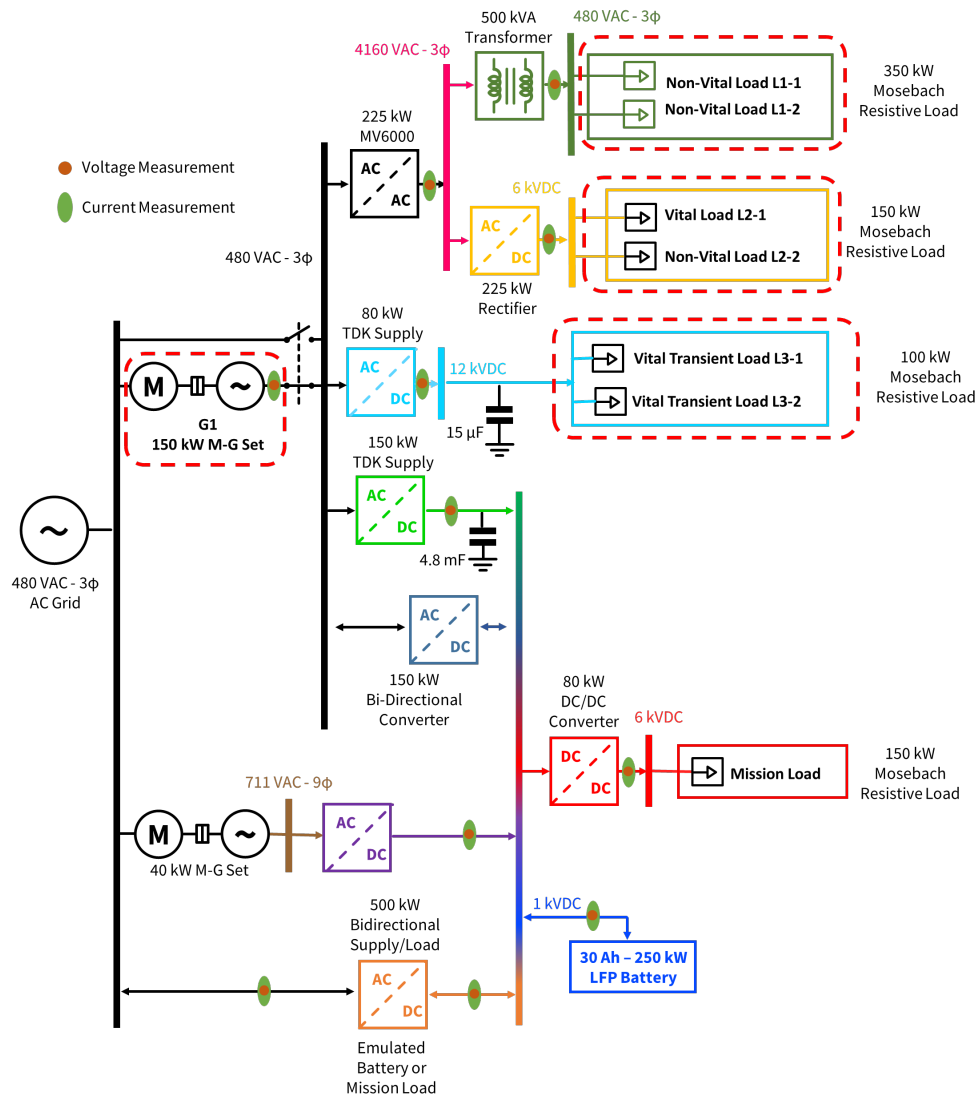


Figure 2. UTA IDEAL testbed one-line diagram.

The M-G set supplies three branches. Two branches are connected to AC/DC converters and one is connected to an AC/AC converter. The interconnection of these four devices forms a point of common coupling (PCC). In Figure 3, the top branch runs from the PCC to a 225 kW GE MV6000 five-level power electronic drive AC/AC converter. Within the MV6000, a step-up eighteen-phase transformer and thirty-six-pulse diode rectifier creates a 6 kV DC link and a five-level IGBT inverter inverts the DC link to generate a three phase 4160 VAC output voltage. Using 0 – 10 V analog reference signals, the output voltage and frequency of the MV6000 can be adjusted between 0.8 p.u – 1.1 p.u. and 50 Hz – 70 Hz, respectively. The MV6000's 4160 VAC output bus is split into two branches, one to a transformer and one into an AC/DC converter. The transformer is a 4160/480 VAC step-down transformer that feeds directly into a 350 kW, 480 VAC resistive load from Mosebach Inc. The load has a 1 kW step resolution controlled either directly on its own control panel or through digital signals supplied by the testbed's control system and emulates traditional shipboard hotel loads (i.e., lighting, heaters, etc.), which typically remain quasi-static once stepped on. In the work presented here, this load is broken up to represent two loads labelled Non-Vital Load L1-1 and Non-Vital Load L1-2. The second branch of the 4160 VAC PCC feeds into an AC/DC rectifier (GE) comprised of an eighteen-phase transformer and thirty-six pulse diode rectifier. This is the same rectifier within the MV6000 creating a 6 kVDC bus voltage loaded by a resistive Mosebach Inc load bank. This bus is typically loaded with a constant load emulating a non-variable baseload. Here, it is treated again as two loads labelled Vital Load L2-1 and Non-Vital L2-2.

The middle electrical branch from the 480 VAC PCC consists of an 80 kW AC/DC converter that takes 480 VAC and converts it to a DC voltage as high as 12 kVDC. This converter is comprised of two capacitive charging power supplies that work in a host-client mode. These capacitor chargers must always be loaded when on, so a 15  $\mu$ F capacitor is floated on the bus for safety. The converter is operated in a current-controlled mode and loaded

using a Mosebach resistive load bank rated as high as 100 kW at 12 kVDC. The current limit of the power supply is controlled using 0 – 10 V analog reference signals supplied by the host controller. Since it is fed into a resistive load, the voltage of the output bus varies as a function of the current. This supply and load are typically used to emulate a high power transient electrical load through modulation of the output current. In this work, it treated as two loads labelled Vital Load L3-1 and Vital Load L3-2.

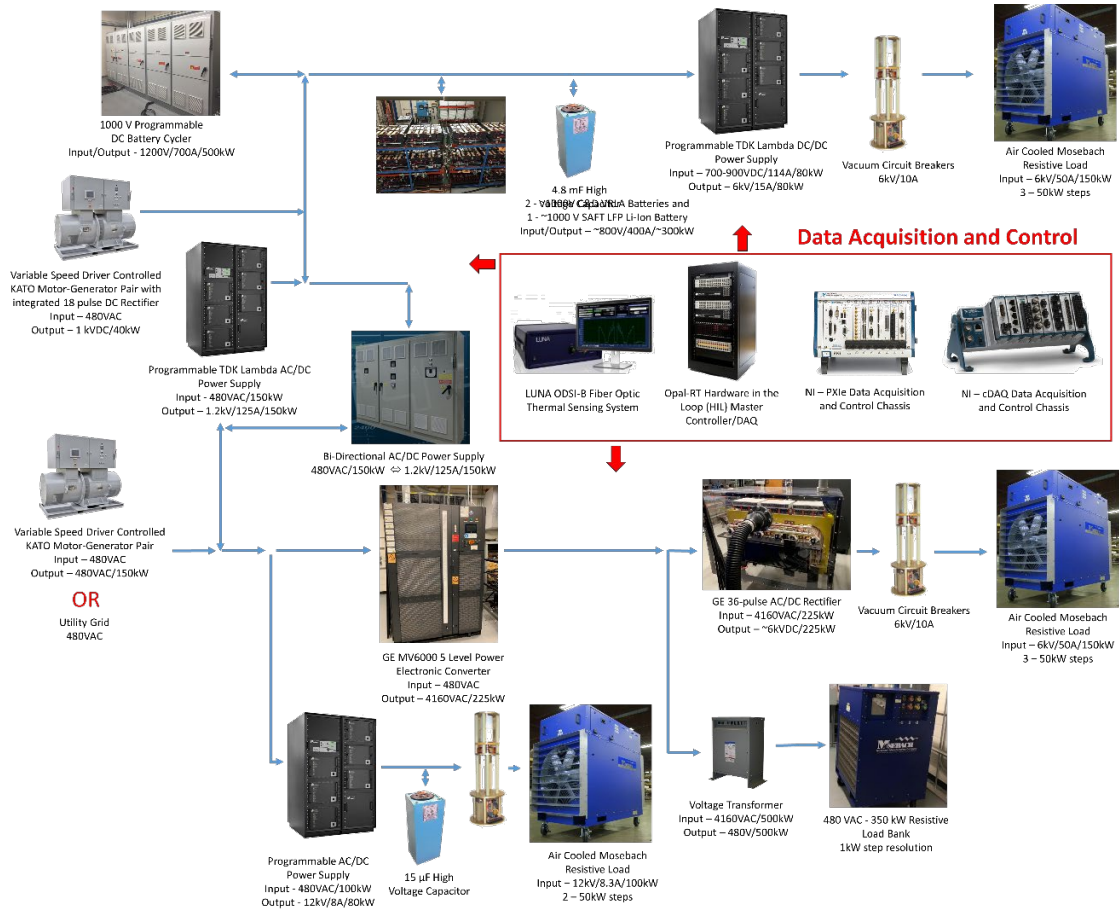


Figure 3. Pictorial one-line diagram of the IDEAL MV DC/AC distributed generation source testbed as it is assembled in the UT Arlington Pulsed Power and Energy Laboratory.

In the lower electrical branch of Figure 2, the 480 VAC PCC supplies an AC/DC power electronic converter feeding a ~1 kVDC PCC. The supply is rated up to 1.2 kVDC and 150 kW with a 4.8 mF capacitor floated on the output bus to protect the supply. The upper branch of the 1 kVDC PCC breaks out to a DC/DC converter that takes the 1 kVDC bus and steps it up to 6 kVDC. This converter is rated at 80 kW loaded using a second 6 kVDC Mosebach resistive load identical to the one installed at the output of the AC/DC rectifier discussed previously. The output current is modulated the same way as the 12 kVDC converter used to emulate a second high power transient load. In this work, it is labelled Mission Load 1. This branch is also supplied by an M-G set that produces 711 VAC with active rectification to 1 kVDC and has a maximum power rating of 40 kW. Though it is not being used in the work presented here, it is a 120 Hz, nine phase synchronous generator with an output voltage and frequency that can be altered by +/- 20% using 0 – 10 VAC inputs or the control panel of the front of the machine. On the lower branch of the 1 kVDC PCC, the LFP battery floats on the bus acting as a buffer. Excess power from the generator is used to charge the battery enabling the system to maintain a base generator load. When power draw exceeds intended base load, the battery supplies the deficiency to the transient 6 kVDC load. The power supplied by the AC/DC converter and the battery is achieved by setting the AC/DC converter's voltage higher than the intended bus voltage and imposing a current limit. Current and voltage setpoints are controlled using analog reference signals supplied by the host controller. All the set points mentioned here are directly controlled using optimization principles and control parameters set by the user in an NI controller. The bi-directional converter between the 480 VAC bus and the 1 kVDC bus was only recently added and once commissioned it will provide enable the battery to be able to buffer any load in the bus instead of only the one 6 kVDC load that it can now.

Finally, between the AC electric grid and the 1 kVDC bus, there is a 500 kW bi-directional power supply/load bank that is able to be used to emulate a power source or act as a non-linear load bank. It is manufactured by Chroma Systems and typically sold as a battery cyclers. It is not used in the work presented here but it has ratings of 1.2 kVDC/ 700 ADC/ 500 kW. Its able to be controlled using analog reference signals in both directions and has a slew rate of roughly 10 ms.

Comprehensive voltage and current measurements are made as indicated in Figure 2. All current measurements are made using closed loop Hall Effect current sensors (Harting 100 A and 300 A sensors) chosen for their 50 kHz bandwidth and 0.5% accuracy. Voltage measurements use one of three types of differential voltage probes: a 1.4 kV, 25 MHz, differential voltage probe manufactured by Pico Technology (model TA057), a 7.0 kV, 70 MHz, differential voltage probe also manufactured by Pico Technologies (model TA044), and a 15.0 kV 50 MHz, differential probe manufactured by Cal . All voltage and current measurements are acquired using an NI PXIe chassis instrumented with data acquisition cards interconnected with the NI cDAQ controller. Network variables are used to pass real-time measurements back to the host system NI LabVIEW control system through an Open Platform Communications United Architecture (OPC-UA) connection for high level control and decision-making. As will be shown, the NI LabVIEW controller communicates with the SLDRT controller developed by CU through a User Datagram Protocol (UDP) connection. The fastest communication rate achieved locally between LabVIEW and SLDRT was approximately 20 ms; however the response time is limited by the loop rate of the SLDRT model. This model interprets and reacts to the larger system every 100 ms which sets the operating time step for the overall system. The UDP packets received by SLDRT contain the real time power consumption of the loads as well as an additional signal giving the operating condition of the generator. The signals to LabVIEW from SLDRT contain a shed command for each load as well as an additional variable to ensure valid data is being sent.

### 3. Advanced Load Shed (ALS) Control Methodology

Referring to the one-line diagram in Figure 2, the testbed loads consist of three different Mosebach units denoted by Load 1 (L1), Load 2 (L2), and Load 3 (L3). L1 is a 480 VAC, 350 kW resistive load that can be stepped in 1 kW steps. L2 is a 6 kVDC, 150 kW load, with a step resolution of 50 kW, that is attached to the output of the rectifier. L3 is an identical load to L2 in capabilities; however, it is used to simulate the transient loads of the system. The motor generator that supplies these loads is only able to source 150 kW at 480 VAC. Note that only the loads listed above, those highlighted in the dashed red boxes in Figure 2, are being used in the work documented here. Thus, without the supplement of the LFP battery, the system max power draw must remain under 150 kW at any given moment. The three loads are subdivided into six distinct loads to be controlled by the user and the load shedding software. For L2 and L3, the two different 50 kW internal steps are treated as separate loads to be enabled, resulting in L2-1, L2-2, L3-1 and L3-2. L1 does not have this same distinction in hardware, but it is programmed to simulate two separate non vital loads. NI's LabVIEW is used to create a GUI to command loads on and off and interfaces with a physical control box that can be used to command supplies and loads as shown in Figure 4.

Clarkson's Advanced Load Shedding (ALS) controller has been tested on IEAL Testbed as shown in Figure 5. The ALS controller consists of three layers: external control, signal communication, and power system hardware. The external control layer is implemented using MATLAB Simulink Desktop Real-Time (SLDRT). The signal communication layer is based on the UDP protocol to exchange UDP data packages between the controller and the LabVIEW power system hardware control system. Finally, the IDEAL testbed is connected to the LabVIEW controller to receive load shedding commands and that controller feeds back the power supplied to each load to the ALS controller.



Figure 4. Main VI used to command supplies and loads in the IDEAL testbed

Figure 6 depicts the specifics of the ALS controller. The supervision system updates IDEAL’s load requirements and system topology, including the status of the generation and energy storage devices. The mission database includes the load prioritization according to the vital nature of the loads. The ALS controller performs the optimization algorithm based on system objectives to generate the load shedding commands for each load during an over-power event. This procedure is repeated every  $T_{con}$  in the real time (RT) operation, where  $T_{con}$  is the control sampling time.

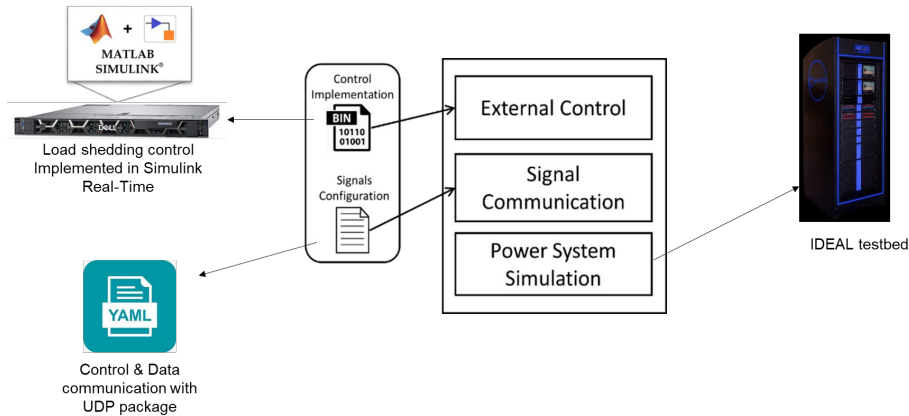


Figure 5. Overall schematic diagram of the ALS controller and IDEAL testbed.

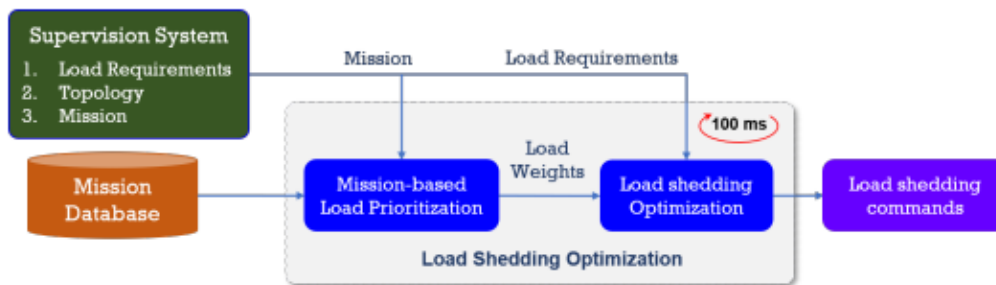


Figure 6. Block diagram of the load shedding control.

The weighting factors ( $\omega_i$ ) represent the load prioritization that the supervision system provides. The degree of load power to be served for each load is quantified by the load operability ( $O$ ) to incorporate the significance of loads and their corresponding rated power in ALS problems, as given by (3.1).

$$O = \frac{\int_{t_0}^{t_f} \sum_{i=1}^{n_L} \hat{\omega}_i o_i^t dt}{\int_{t_0}^{t_f} \sum_{i=1}^{n_L} \hat{\omega}_i o_i^{*t} dt}, \quad (3.1)$$

where  $n_L$  is the number of loads;  $P_i^{L, rated}$  is the rated power of load  $i$ ;  $\hat{\omega}_i$  is the normalized weight value of load  $i$  as defined in (3.2);  $o_i^t$  is the operational status of load  $i$  at time  $t$ ;  $o_i^{*t}$  is the commanded operational status of load  $i$ ;  $t_0$  represents the start time of the operation, and  $t_f$  represents the end time of the operation.

$$\hat{\omega}_i = \omega_i P_i^{L, rated}, \forall i \in n_L. \tag{3.2}$$

The formulation of the ALS problem is based on load weights ( $\omega_i$ ) and the load demand to determine how much load to shed. The operational status ( $o_i$ ) indicates the operability of load  $i$  and is the optimal variable of the optimization problem. For instance,  $o_i = 0$  means load  $i$  will be shed 100%;  $o_i = 1$ , means load  $i$  will be served 100%.

The primary objective of the ALS is to maximize total load operability, which is demonstrated by the ALS objective function in (3.3a). The controller’s formulation was leveraged from Clarkson previous work in (Xing 2012) with the following modification, which considers ramp-rate of load devices for a more effective load shedding mechanism.

$$\max_{o_i} \frac{\sum_{i=1}^{n_L} \hat{\omega}_i o_i}{\sum_{i=1}^{n_L} \hat{\omega}_i o_i^*} \tag{3.3a}$$

subject to:

$$\sum_{i=1}^{n_L} P_i^{L*} o_i \leq (1 - \beta) \sum_{g=1}^{n_G} P_g^G, \tag{3.3b}$$

$$r_L^{min} \leq \Delta P_i^L \leq r_L^{max} \quad \forall i \in n_L, \tag{3.3c}$$

$$\Delta P_i^L = P_i^{L*} o_i - P_i^{Lp} o_i^p \quad \forall i \in n_L, \tag{3.3d}$$

$$0 \leq o_i \leq 1 \quad \forall i \in n_L. \tag{3.3e}$$

$$o_i \in \begin{cases} Z \\ [0,1] \end{cases} \quad \text{if load } i \text{ is the step load,} \\ \text{otherwise.} \tag{3.3f}$$

where  $n_G$  is the number of generators;  $\beta$  is the percentage of reserved power;  $P_i^{L*}$  is the reference of load  $i$ ;  $P_i^{Lp}$  is the load data from previous interval state;  $r_L^{min}$  and  $r_L^{max}$  are the minimum and maximum ramp-rate of loads; where  $Z = \{0: \Delta o_i: 1\}$ ;  $\Delta o_i = 1/n$ ;  $n \in Z^+$  is the number of steps of the load command.

The objective function is subjected to the generation-demand constraint (3.3b) to ensure that the total load command is smaller than the total available generation. Constraint (3.3c) indicates the ramp-rate limit of loads. The operational status is subjected to the limit constraints (3.3e). Finally, since some loads are discrete changes, the operational status of such loads is subject to the constraint of the discrete function (3.3f.)

#### 4. Experimental Results

The ALS controller has been tested here on the IDEAL Testbed, with the loads defined as they are in Figure 2. The control sampling time of the ALS control ( $T_{con}$ ) is 100 ms. One generator with a total capability of 150 kW is used to supply power to loads. It is assumed that this generator is always available, and it can supply up to 95% of its capability with 5 percent held in reserve. The generator and load parameters are defined in Table 1. There’re six loads in the system. Non-Vital Load L1-1 and Non-Vital Load L1-2 have rated power levels of 5 and 10 kW, respectively. They are stepped loads and their power is adjusted at a step-size of 1 kW (for example: 1 kW, 2 kW, etc.) Vital Load L2-1 and Non-Vital Load L2-2 are in zone 2 and each has a rated power of 50 kW. As a specific requirement of Vital Load L2-1, it must be always operated at full capacity. The ALS control can guarantee to meet this requirement by putting a high value of load priority factor. Non-Vital Load L2-2 is a binary load, which only turns on or off. The last two loads, namely Vital Load L3-1 and Vital Load L3-2 have rated power levels of 15 kW and 40 kW, respectively. Those loads are the same type as Non-Vital Load L1-1 and Non-Vital Load L1-2 but with a step size of 0.25 kW.

Table 1. Parameters of loads and generator

	Name	Rated power (kW)	Load weights	Step Load Value
<b>Generator</b>	G1	150	-	-
<b>Loads</b>	Non-vital L1-1	5	0.2	Step-size of 1 kW
	Non-vital L1-2	10	0.2	Step-size of 1 kW

	Name	Rated power (kW)	Load weights	Step Load Value
Generator	G1	150	-	-
	Vital L2-1	50	High value	Always ON
	Non-vital L2-2	50	0.2	Binary load (0/1)
	Vital L3-1	15	0.5	Step-size of 0.25 kW
	Vital L3-2	40	0.5	Step-size of 0.25 kW

Prior to implementation on the IDEAL hardware, the ALS was simulated using SLDRT. Because it is a simulation, it is not bound to the hard step requirements the hardware is and therefore the load shed is variable. Figure 7 depicts the load profile of the six loads during a 315 s long simulation. From the beginning to 80 s, all loads have small load demands compared to their rated power. From 80 s to 315 s, their power demands increase gradually, eventually exceeding the available power from the generator.

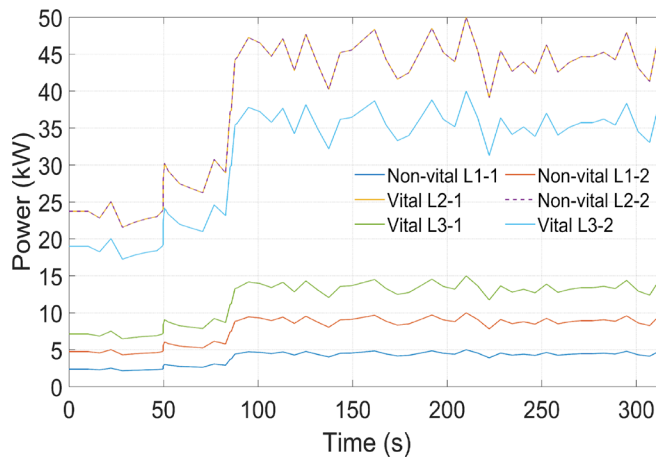


Figure 7. Load profile

Figure 8 and Figure 9 show the control performance of ALS in the overload condition. Figure 8 shows the total load demanded from the generator G1 while Figure 9 shows the load commanded to be shed. From the beginning to 80 s, all loads are served as the total generation is larger than the load demand. As seen in Table 1, the weight of Vital Load L3-1 is higher than Non-Vital Loads Zone 1 and equal to Vital Load L3 – 2. Since the controller takes into account not only the weight factor but also the rated power, the reduction in Vital Load L3 – 2, which has a higher rated power would improve the overall system operability. Therefore, we recommend future designs of the weighting factor would need to be considered together with the rated power to avoid such an issue. At 80 s, the load demand gradually increases, which triggers the ALS control to shed loads to maintain the power balance. At 80 s, when the load first exceeds the rating of the generator, Vital Load L3 – 2 is periodically shed to reduce the generator load. as well as to improve the overall operability of the system. Vital Load L2-1 always remains on while Non-Vital Load L2-2 is shed a few times, the first beginning at approximately 160 s and the second at approximately 190 s to reduce the total load power.

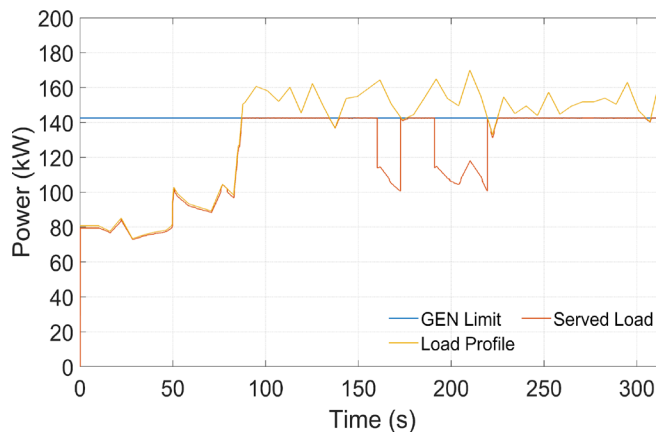


Figure 8. Load shedding during shortage power

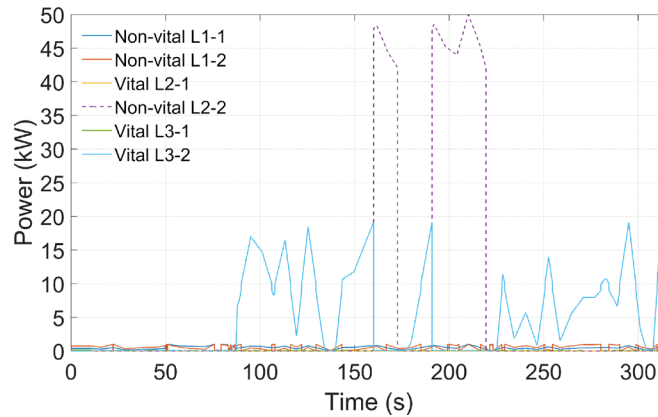


Figure 9. Load shedding commands

Figure 10 shows experimental results obtained when the ALS is implemented on the IDEAL testbed. In the experiment, Vital Load L2-1 and Non-Vital Load L2-2 are powered on, drawing ~100 kW from the system. Non-Vital Load L1-1 and Non-Vital Load L1-2 are stepped on together, when the user presses buttons on the control box, until the demand reaches approximately 145 kW at ~854 s. Once 145 kW load demand is reached, the ALS instructs the LabVIEW controller to shed Non-Vital Load L1-1, bringing the generator back into acceptable range. Three instances of the ALS shedding Non-Vital Load L1-1 are seen in the figure. User requested increases and decreases in Non-Vital Load L1-2 are seen in the rightmost plot of Figure 10. Each time the user's requests push the generator power up to, or more than, 145 kW, the ALS is engaged. Note there are user requested decreases in Non-Vital Load L1-1 that occur just after 865 s that are not ALS induced.

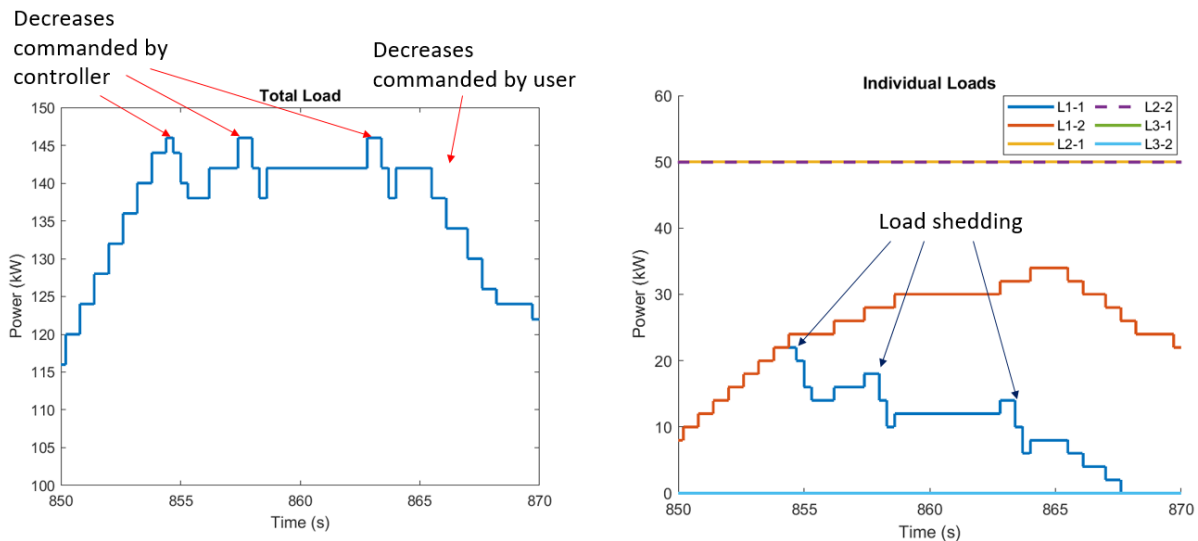


Figure 10. Load shedded by SLDRT controller. Load step 1 and two are increased until 145kW is reached. An increase in the load after this results in the controller shedding power of L1-1 while L1-2 is allowed to increase.

Though brief, the experiment on IDEAL demonstrates the successful communication of the ALS with the IDEAL LabVIEW controller. Latencies between 100 ms and 200 ms have been measured between the two control systems and while the goal is always to reduce that, it does appear to be sufficient so far for keeping the load on the generator below 145 kW. Soon, the plan is to continue to introduce the additional hardware elements that are not utilized in the experiments discussed here. They will be assigned their own weighting and priority similar those already described. Finally, there is a plan to introduce ramp rate support using the lithium-ion energy storage so that the generator is not subjected to transient loading. Variation of the ramp rate according to the power supply's current mode of operation and load priority.

## 5. Conclusions

In this report, the design and construction of the UTA Intelligent Distributed Energy Analysis Laboratory (IDEAL) has been presented along with a demonstration of how an advanced load shedding algorithm has been implemented to ensure the primary generation source never exceeds its rated power capability. The testbed was designed as a platform on which the integration and controls challenges that future shipboard distributed power

system engineers will face can be studied and better understood. This work is just a first step in the work that is planned. The demonstration here has shown that latencies as high as 200 ms have been observed but found to be adequate for protecting the generator and maintaining the intended load. The prioritization algorithm has been demonstrated and will continue to be expanded as additional hardware not used to date is introduced into it.

### Acknowledgements

The authors would like to thank ONR for their financial support of this effort through grants N00014-18-1-2714, N00014-16-1-2956, and N00014-21-1-2239. Any opinions and findings are those of the authors and not those of ONR or NSWC-Philadelphia.

### References

- J.F. Hansen and F. Wendt, 'History and State of the Art in Commercial Electric Ship Propulsion, Integrated Power Systems, and Future Trends,' Proceedings of the IEEE | Vol. 103, No. 12, December 2015.
- G. Ortiz, J. Biela, D. Bortis, J.W. Kolar, "1 Megawatt, 20 kHz, Isolated, Bidirectional 12 kV to 1.2 kV DC-DC Converter for Renewable Energy Applications," The 2010 International Power Electronics Conference – ECCE ASIA, IEEE, 2010.
- ONR Electric Ship Research Development Consortium, <https://www.esrdc.com/>, Online August 19, 2021.
- U. Javaid, D. Dujic, W.V.D. Merwe, "MVDC Marine Electrical Distribution: Are we ready?," IECON 2015 – 41st Annual Conference of the IEEE Industrial Electronics Society, IEEE, 2015.
- Next Generation Integrated Power System, NGIPS Technology Development Roadmap, Ser 05D / 349, November 30, 2007.
- Z. Ding, S. K. Srivastava, D. A. Cartes and S. Suryanarayanan, "Dynamic Simulation Based Analysis of a New Load Shedding Scheme for a Notional Destroyer Class Shipboard Power System," 2007 IEEE Electric Ship Technologies Symposium, 2007, pp. 95-102, doi: 10.1109/ESTS.2007.372070.
- H. Ravindra, J. Langston, and K. Schoder, 'Model Design Document, System Model for RCPC Demonstration 1, DCN# 43-9757-22, [https://www.esrdc.com/media/1110/demo1\\_system\\_mdd\\_distroa.pdf](https://www.esrdc.com/media/1110/demo1_system_mdd_distroa.pdf), [ONLINE], Accessed 7-11-2022.
- Z. Ding, S. Srivastava and D. Cartes, "Expert System based Dynamic Load Shedding Scheme for Shipboard Power Systems," Conference Record of the 2006 IEEE Industry Applications Conference Forty-First IAS Annual Meeting, 2006, pp. 1338-1344, doi: 10.1109/IAS.2006.256704.
- S. Xing, "Microgrid emergency control based on the stratified controllable load shedding optimization," International Conference on Sustainable Power Generation and Supply (SUPERGEN 2012), 2012, pp. 1-5, doi: 10.1049/cp.2012.1778.
- B. L. H. Nguyen et al., "Advanced Load Shedding for Integrated Power and Energy Systems," 2021 IEEE Electric Ship Technologies Symposium (ESTS), 2021, pp. 1-6, doi: 10.1109/ESTS49166.2021.9512317.
- M. Sabah, I. T. Ojo and A. M. Cramer, "Evolution of Operability-Based Performance Metrics for Assessment of Mission Performance," 2021 IEEE Electric Ship Technologies Symposium (ESTS), 2021, pp. 1-6, doi: 10.1109/ESTS49166.2021.9512362.
- A.N. Johnston, Z.R. Bailey, D.A. Wetz, G.K. Turner, and J.M. Heinzl, 'Design and Commissioning of a Medium Voltage Testbed with Emulated Pulsed Loads,' Accepted for publication in the Naval Engineers Journal, March 2022, publication pending.
- A.N. Johnston, D.A. Wetz, R. Madani, A. Davoudi, G.K. Turner, D.A. Dodson, B.J. McRee, Z. Bailey, D. Pullaguram, J.M. Heinzl, M. Giuliano, and C.M. Schegan, 'Mitigating Transient Loads in Medium-Voltage Direct Current Microgrids,' Proceedings of the 2020 American Society of Naval Engineers (ASNE) Advanced Machinery Technology Symposium (AMTS), October 7-8, 2020, Philadelphia, Pennsylvania.
- A.N. Johnston, D.A. Wetz, Z. Bailey, D.A. Dodson, B.J. McRee, and J.M. Heinzl, 'A Medium Voltage, Distributed Power Generation Testbed Deploying Transient Loads,' Proceedings of the International Ship Control Systems Symposium (iSCSS), October 6 – 8, 2020, Delft, Netherlands.

A.N. Johnston, G.K. Turner, D.A. Wetz, Z.R. Bailey, C. Schegan, J.M. Heinzl, and M. Giuliano, 'Emulation of a Single Zone of an Integrated Power System,' American Society of Naval Engineers (ASNE) Intelligent Ships Symposium (ISS), April 28 – 29, 2021, VIRTUAL.